Collagen and Leather

RESEARCH Open Access

Bioactive poly(ethylene glycol)-chondroitin sulfate-triple helical recombinant collagen hydrogel for enhanced cranial defect repair

Lili Wang[1,2,3†], Shanshan Zhang[1,4†], Fan Yang[1†], Xian Chen[1,2,3], Huixia He[1,2,3], Zaiman Liu[4] and Jianxi Xiao[1,2,3*]

Abstract

The reconstruction of critical-size calvarial defects remains a fundamental challenge. Recombinant collagen has gained significant attention in bone tissue engineering owing to its remarkable bioactivity and non-immunogenicity. Herein, we have for the first time developed a bioactive poly(ethylene glycol)-chondroitin sulfate-triple helical recombinant collagen (PEG-ChS-THRC) hydrogel for enhanced bone regeneration in cranial defects. A simple and mild crosslinking reaction of two-arm polyethylene glycol active ester (NHS-PEG-NHS), adipic dihydrazide modified chondroitin sulfate (ChS-ADH) and triple helical recombinant collagen (THRC) leads to the formation of the PEG-ChS-THRC hydrogel. The hydrogel demonstrates interconnected porous structures, enhanced mechanical strength, diminished swelling ratios and adjustable biodegradability. It possesses exceptional biocompatibility and bioactivity, significantly facilitating cell proliferation, adhesion, migration, and osteogenic differentiation of BMSCs. Micro-computed tomography (micro-CT), magnetic resonance imaging (MRI) and histological characterization of rat models with critical-size cranial defects have consistently demonstrated that the PEG-ChS-THRC hydrogel significantly promotes bone tissues regeneration. The innovative bioactive scaffold provides a remarkably improved remedy for critical-size cranial defects, holding greatly promising applications in the fields of bone tissue regeneration.

Keywords Bioactive, Recombinant collagen, Hydrogel, Cranial defect repair

† Lili Wang, Shanshan Zhang and Fan Yang contributed equally to this work.

*Correspondence:
Jianxi Xiao
xiaojx@lzu.edu.cn
Full list of author information is available at the end of the article

Graphical Abstract

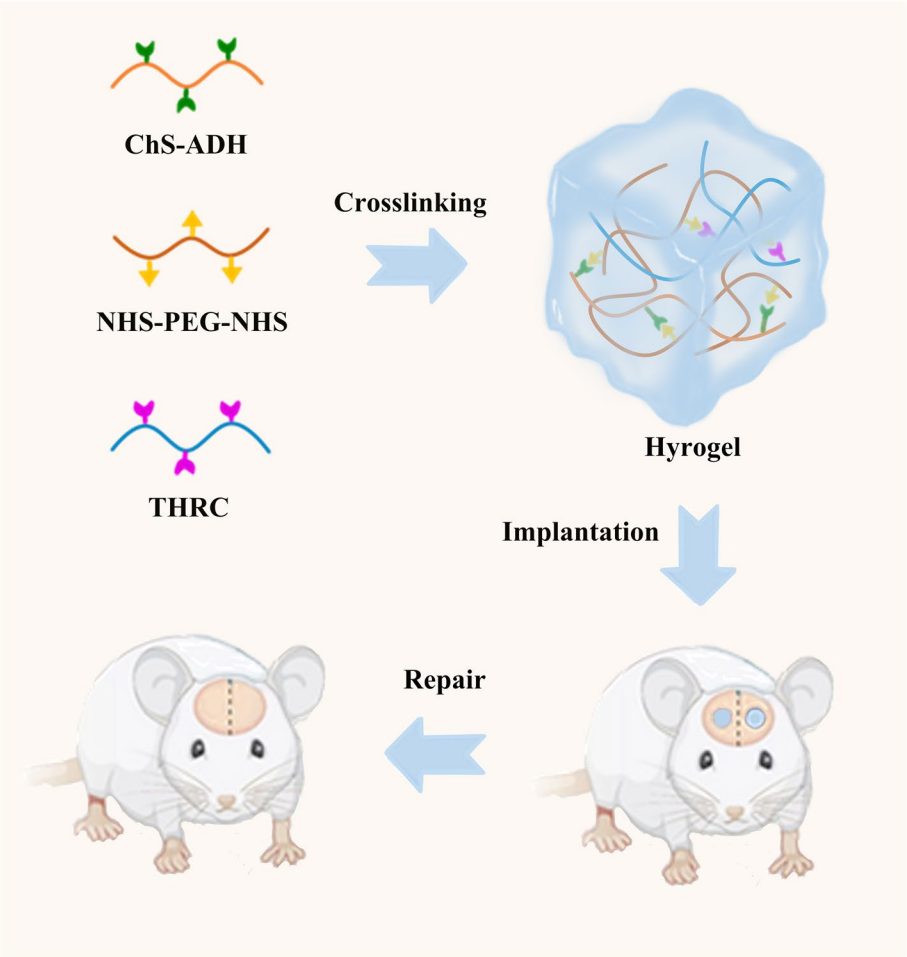

1 Introduction

Calvarial defects pose significant reconstructive challenges stemming from various etiologies, including traumatic brain injury, cerebrovascular disease, oncologic resection, and congenital anomalies [1, 2]. Despite the innate regenerative potential of craniofacial bone, it is incapable of spontaneously repairing significant or critical-sized defects [3]. Current surgical interventions involving autografts and allografts are hindered by significant drawbacks, including limited accessibility, donor site morbidity, pathogen transmission, and immunological rejection [4–6]. Commonly used substitutes, such as titanium mesh and polyether ether ketone, suffer from poor osteointegration and limited biologic activity [7].

Hydrogels have garnered significant attention as scaffolds for tissue engineering to address calvarial defects, owing to their adaptable physicochemical properties [8–10]. Poly(ethylene glycol) (PEG) has been extensively employed in the fabrication of hydrogels due to its superior mechanical characteristics [11, 12]. Poly(ethylene glycol)-diacrylate and poly(ethylene glycol)-dithiothreitol hydrogels have been investigated for the treatment of calvarial defects [13, 14]. Nevertheless, their subpar biocompatibility and limited biodegradability may potentially hinder their therapeutic effectiveness. Various natural polymers, such as chondroitin sulfate and sodium alginate, have been integrated into poly(ethylene glycol) hydrogel to modulate its structural, mechanical, and biological attributes [15, 16]. However, the intricate preparation process and constrained bioactivity might restrict their clinical utility.

Collagen, the principal constituent of natural bone, has been explored for the fabrication of these hydrogels thanks to its remarkable biocompatibility, exceptional

bioactivity, and suitable biodegradability [17–19]. Unlike the traditional utilization of animal-derived collagen, recombinant collagen presents notable advantages, encompassing non-immunogenicity, diminished risk of viral infection, and consistent quality [20–22]. Nevertheless, the advancement of recombinant collagen-based hydrogel for cranial defect repair has scarcely been reported.

Herein, we have for the first time developed a bioactive poly(ethylene glycol)-chondroitin sulfate-triple helical recombinant collagen (PEG-ChS-THRC) hydrogel for enhanced cranial defect repair. The PEG-ChS-THRC hydrogel was fabricated via a simple crosslinking strategy of two-arm polyethylene glycol active ester (NHS-PEG-NHS), adipic dihydrazide modified chondroitin sulfate (ChS-ADH) and triple helical recombinant collagen (THRC). The hydrogel displayed various adjustable properties including porous structure, mechanical strength, swelling ratios and degradation of collagenase, while also exhibiting a remarkable ability to enhance cell proliferation, adhesion, and osteogenic differentiation of BMSCs. In rat models of critical-size cranial defects, the PEG-ChS-THRC hydrogel has significantly accelerated cranial regeneration compared with poly(ethylene glycol)-chondroitin sulfate (PEG-ChS) hydrogels. This advanced hydrogel provides a highly efficient treatment of critical-size cranial defects, suggesting its potential applications in the realms of orthopedics and plastics.

2 Experimental section

2.1 Materials

Chondroitin sulfate (ChS, 50–100 kDa) was purchased from Sangon Biotech (Shanghai, China). Adipic acid dihydrazide (ADH) and N-hydroxysuccinimide (NHS) were obtained from Xiya Reagent (Chengdu, China). 1-(3-dimethylaminopropyl)-3-ethylcarbodiimide hydrochloride (EDC) was procured from Aladdin (Shanghai, China). Two-arm polyethylene glycol active ester (NHS-PEG-NHS, 10 kDa) with substitution (^{1}H NMR) -NHS of 98% was acquired from Ponsure Biotechnology (Shanghai, China). Sodium hydroxide was purchased from Tianjin Damao Chemical Reagent Factory. Sodium dihydrogen phosphate and disodium hydrogen phosphate were obtained from Sinopharm Chemical Reagent Co., Ltd.

2.2 Preparation and characterization of THRC

Triple helical recombinant collagen (THRC) was expressed in the *E. coli BL21* strain according to established protocols [23]. In brief, *E. coli* cells were seeded in the 50 mL Luria-Bertani media augmented with 100 μg/mL ampicillin overnight at 37 °C, and subsequently scaled up to 1 L Luria-Bertani media. When the OD_{600nm} of the media reached 0.8, the addition of isopropyl beta-D-thiogalactopyranoside (IPTG, 1 mM) was employed to induce protein expression at 25 °C. After overnight incubation, the collected *E. coli* cells were resuspended in 20 mM sodium phosphate buffer (pH 7.4) containing 0.5 M NaCl and 30 mM imidazole, and underwent ultrasound-induced disruption. The harvested supernatant was subjected to Ni-NTA-Sepharose column purification with 20 mM sodium phosphate buffer (pH 7.4) including 0.5 M NaCl and 0.5 M imidazole. The purified protein underwent trypsin digestion at 28 °C for 24 h and was subsequently dialyzed against 20 mM PBS buffer (pH 7.4). The resulting THRC was lyophilized and stored at -20 °C for future applications.

The purity of THRC was validated through sodium dodecyl sulfate-polyacrylamide gel electrophoresis (SDS-PAGE). Circular dichroism (CD) spectra were acquired using a J1500 spectrophotometer (JASCO, Japan). Wavelength scans spanning 190 to 300 nm were registered at 4 °C, with a precision of 0.5 nm per increment. The thermal transition was discerned by measuring the intensity of the CD peak at 225 nm, as the temperature increased gradually from 5 to 60 °C. The heating protocol maintained an average rate of 0.5 °C/min, and an equilibration period of 2 min. The determination of the melting temperature (Tm) was derived from the extrema of the first derivative.

2.3 Synthesis and characterization of ChS-ADH

The chondroitin sulfate-adipic dihydrazide (ChS-ADH) was synthesized following a previously reported method [24]. Briefly, 1 g chondroitin sulfate (ChS) was dissolved in 500 mL of ultrapure water, and thoroughly blended with 0.47 g EDC and 0.35 g NHS. The mixture was incubated for 30 min after adjusting the pH to 5.5 by dropwise addition of HCl. Subsequently, 3.2 g of ADH was added, and the pH was readjusted to 6.0 with NaOH. The resulting mixture was shaken at room temperature for 24 h. The resulting ChS-ADH was dialyzed, lyophilized and stored at -20 °C for future use. The modification level of ChS by ADH was determined by ^{1}H NMR spectra in deuterium oxide (D_2O) using a JNM-ECS400M Spectrometer (JEOL, Japan).

2.4 Preparation and characterization of PEG-ChS and PEG-ChS-THRC hydrogels

NHS-PEG-NHS and ChS-ADH were dissolved as 160 mg/mL and 100 mg/mL solutions in 0.9% saline, respectively. 500 μL of NHS-PEG-NHS were mixed with 500 μL of ChS-ADH, and gently stirred at room temperature. PEG-ChS hydrogel was formed after incubation for 15 min. Additionally, 20 mg, 40 mg, and 80 mg of lyophilized THRC were dissolved in the 500 μL of 100 mg/

mL ChS-ADH solution, yielding a series of mixtures of ChS-ADH and THRC. 500 μL of 160 mg/mL NHS-PEG-NHS solution was added to the mixtures of ChS-ADH and THRC, and ultimately resulting in the formation of PEG-ChS-$THRC_{10}$, PEG-ChS-$THRC_{20}$, and PEG-ChS-$THRC_{40}$ hydrogel after incubation for 15 min at room temperature.

Fourier transform infrared (FT-IR) spectroscopy was conducted using a Nicolet NEXUS 670 FTIR spectrometer ranging from 400 to 4000 cm^{-1}. The freeze-dried samples, including ChS, THRC, ChS-ADH, NHS-PEG-NHS, and PEG-ChS-THRC, were mixed and ground with KBr in a mass ratio of 1:100, respectively. The resulting homogeneous powders were then compressed into a transparent sheet using a tablet press for subsequent FTIR analysis.

The morphology of the PEG-ChS and PEG-ChS-THRC hydrogels was examined with a Hitachi S-4800 scanning electron microscope (Hitachi Limited, Japan) operating at 5.0 kV. To enhance conductivity, the freeze-dried hydrogels were meticulously positioned in an ion sputterer (Hitachi, Japan) for gold spraying before imaging. The pore sizes for freeze-dried hydrogels were analyzed using Image J software, with a mean value of three images.

Rheological tests were carried out using an Anton Paar rheometer at room temperature. The PEG-ChS, PEG-ChS-$THRC_{10}$, PEG-ChS-$THRC_{20}$, and PEG-ChS-$THRC_{40}$ hydrogels were prepared respectively, and then placed in the center of a 15 mm diameter parallel plate. Frequency-dependent rheological behaviors were examined through oscillation frequency measurements with a 1% strain, while strain-dependent oscillatory rheology was performed at a 1 Hz frequency.

The lyophilized hydrogel specimens (PEG-ChS, PEG-ChS-$THRC_{10}$, PEG-ChS-$THRC_{20}$, and PEG-ChS-$THRC_{40}$) were initially weighed (m_0, g) and subsequently immersed in a PBS solution. At designated time intervals, the specimens were extracted from the PBS solution, eliminated surplus water, and then re-weighed (m_t, g). The swelling rate (SR) was calculated employing the equation: SR (g/g) = (m_t - m_0) / m_0.

The freeze-dried hydrogels (PEG-ChS, PEG-ChS-$THRC_{10}$, PEG-ChS-$THRC_{20}$, and PEG-ChS-$THRC_{40}$) were initially weighed (m_0, mg) and subsequently exposed to a TES buffer (1mM $CaCl_2$, pH 7.4) containing 10 U/mL of collagenases at 37 ℃, respectively. To uphold consistent enzyme activity, the collagenase solution underwent replacement once daily. At various time intervals, the specimens were extracted from the collagenase solution and rinsed thrice with deionized water. The residual weights (m_t, mg) of the specimens were determined after freeze-drying. The mass degradation percentage (MD, %) was computed using the equation: MD (%) = (m_0 - m_t) / $m_0 \times 100\%$.

2.5 Cell experiment of PEG-ChS and PEG-ChS-THRC hydrogels

The second generation of rat bone marrow mesenchymal stem cells (rBMSCs, P2) were obtained from the Cell Bank of the Chinese Academy of Science (Shanghai, China), and cultured in α-MEM medium (15% FBS, 1% penicillin-streptomycin antibiotics) at 37 °C in a 5% CO_2 atmosphere. The adherent cells were dissociated into suspension using 0.25% (w/w) trypsin.

100 μL of rBMSCs suspension (1×10^6 cells/mL) were added to a 96-well plate and incubated for 24 h. After removing the culture medium, 100 μL of the extract of PEG-ChS and PEG-ChS-THPC hydrogels were added to the wells, while the blank group received α-MEM medium. Following a 24-hour incubation at 37 °C, 10 μL of CCK-8 was added to each well, and the cells were cultured for another 30 min at 37 °C. The absorbance at 450 nm was measured using a Tecan Infinite F200/M200 multifunctional microplate reader (Tecan, Mannedorf, Switzerland).

100 μL of rBMSCs suspension with a density of 1×10^5 cells/mL were added to a 96-well plate and cultured in cell incubator for 24 h. Subsequently, 100 μL of hydrogel samples diluted 100 times were added to their respective wells, while the fresh α-MEM medium was supplemented into the blank group. After incubation of 1, 3, and 7 days, 10 μL of CCK-8 was added into each well, and then cultured at 37 °C for another 30 min. The absorbance at 450 nm was measured using a Tecan Infinite F200/M200 multifunctional microplate reader (Tecan, Mannedorf, Switzerland).

The mixture comprising rBMSCs and hydrogel (diluted 100 times) at a density of 1×10^5 cells/mL was cultured in a laser confocal dish. Following 7 days of incubation, the cells underwent fixation in 4% paraformaldehyde for 15 min, permeabilization with 0.1% Triton X-100 for 5 minutes, and blocking using a 1% BSA solution for 30 min at room temperature. Phalloidin-tetramethylrhodamine isothiocyanate (Solarbio, China) and Hoechst 33,258 (Solarbio, China) were employed to stain F-actin and cell nuclei at 37 ℃, respectively. Ultimately, fluorescence images were acquired using laser confocal microscopy (Olympus, FV3000, Japan).

Three horizontal lines, spaced at intervals of 0.5^{-1} cm, were drawn along the bottom of a 6-well plate using a marker pen. rBMSCs with a density of 1×10^6 cells per well were cultured at 37 °C for 24 h. Cell scratches were created vertically along the horizontal lines at the bottom using a 10 μL pipette tip. After being rinsed with PBS, 2 mL of hydrogel samples diluted 100 times were

added into separate wells, followed by an incubation period at 37 °C for 24 h. The images of cell scratches were captured at 0 and 24 h using an inverted microscope (Olympus, IX53, Japan).

The suspension of BMSCs and diluted hydrogels with a density of 1×10^5 cells/mL were added into the 6-well culture plates, and then incubated for 1, 3 and 7 days, respectively. Subsequently, total RNA was extracted using an RNA isolation kit (Accurate Biology, AG21101, China). The expression levels of genes were analyzed using PrimeScript RT reagent Kit with gDNA Eraser (Takara, Japan) and TB Green Premix Ex Taq II (Takara, Japan) as well as Real-Time PCR System (Agilent, Mx 3005P, USA). The relative expression level of the target genes was calculated by the $2^{-\Delta\Delta CT}$ method, which was normalized to the expression of a housekeeping gene (β-actin). The changes of osteogenic genes were relative to the blank group at day 1. The primer sequences of osteogenic genes are listed in Table 1.

2.6 Animal model construction and in vivo implantation

The animal study was approved by the Ethics Committee of the Lanzhou University No.1 Hospital (No. LDYYLL-2019-271). All the animals were purchased from Laboratory Animal Center of Lanzhou University and the animal certification is No. LZU-SD-1206-30. Prior to surgery, male SPF Sprague Dawley (SD) rats (250-300 g) were anesthetized with a 10% (w/v) sodium pentobarbital intraperitoneal injection (0.3 mL/100 g). The surgical site was shaved and sterilized with iodophor for aseptic conditions. A midline linear incision on the scalp was made to expose the cranial bone, and two calvarial defects with 5 mm diameter were meticulously created using a dental drill. Subsequently, PEG-ChS and PEG-ChS-THPC hydrogels (5 mm diameter, 2 mm thickness) were respectively implanted into the calvarial defect sites ($n=8$). Both calvarial defects of each rat were filled with the identical hydrogel. Control groups ($n=8$) received no interventions before the wounds were sutured. At different time intervals, rats of each group were euthanized by an overdose of sodium pentobarbital.

Table 1 Primer sequences of osteogenic genes for RT-qPCR

Gene	Forward (5′-3′)	Reverse (5′-3′)
ALP	AACCTGACTGACCCTTCCCTCT	TCAATCCTGCCTCCTTCCACTA
Col1a1	GCTTGGTCCACTTGCTTGAAGA	GAGCATTGCCTTTGATTGCTG
Runx-2	AGTAAGAAGAGCCAGGCA GGTG	GTGTAAGTGAAGGTGGCT GGATAG
β-actin	CCCATCTATGAGGGTTACGC	TTTAATGTCACGCACGATTTC

2.7 CT and MRI characterization

CT experiments were conducted using a dual-source CT scanner (SIEMENS SOMATOM Definition Flash). The X-ray source voltage was fixed at 120 kVp, and the tube current was maintained at 5 mA. Image data (image matrix $480\times480\times636$) were reconstructed employing a modified Feldkamp algorithm with a voxel size of 0.2 mm^3. The volumetric scanning technique was utilized, with a total scan time of 3 mins, an exposure time of 2 s, and a spiral scan pitch of 0.6 mm. The analysis of the defect areas was conducted utilizing CT-analyzer software, with the mean value derived from four images.

MRI scans were executed on a MAGNETOM Skyra 3.0 T magnetic resonance imaging system. T1-weighted experiments utilized the SE sequence with a TE of 9 ms, TR of 500 ms, FOV of 100×100 mm, and a slice thickness of 1 mm. T2-weighted experiments were performed employing the SE sequence with a TE of 106 ms, TR of 3000 ms, FOV of 80×80 mm, and a slice thickness of 1.5 mm. T2-tirm experiments were conducted using the TSE sequence with a TE of 86 ms, TR of 8000 ms, FOV of 80×80 mm, and a slice thickness of 1 mm.

2.8 Histological analysis

The collected cranial bone samples underwent fixation in 4% paraformaldehyde for 48 h, followed by decalcification in a Rapid Cal-Immuno decalcification solution for one week. Subsequently, the samples underwent dehydration through a gradient of alcohol, paraffin embedding, and were then sectioned into 8 μm slices. Standard Hematoxylin-Eosin (H&E) staining protocols were applied to these tissue slices. The sections underwent dewaxing using a xylene solution, followed by dehydration using gradient alcohols and immersion in water. Subsequently, the slices were stained with a hematoxylin solution for 15 min and immersed in a differentiation solution for 3 min, followed by rinsing in running tap water. Re-staining was performed using an eosin solution for 2 min, followed by dehydration in gradient alcohols. Finally, the specimens were rendered transparent using xylene and sealed with resinene. Analysis of all histological sections was conducted using a digital image analysis system (Nikon E 600 Microscope with a Nikon Digital Camera DXM 1200, Nikon Corporation, Japan).

2.9 Statistical analysis

The data were presented as the mean ± standard deviation (SD) of three experiments and statistically analyzed by Student's t-test. Statistical significance was defined as $^{*}P<0.05$, $^{**}P<0.01$ and $^{***}P<0.001$, respectively.

3 Results and discussion

3.1 Design of PEG-ChS-THRC hydrogel

A bioactive poly(ethylene glycol)-chondroitin sulfate-triple helical recombinant collagen (PEG-ChS-THRC) hydrogel has been constructed for enhanced cranial defect repair (Fig. 1). ChS-ADH was initially synthesized through a condensation reaction involving the amine groups in adipic dihydrazide (ADH) and the carboxyl groups in chondroitin sulfate (ChS). The molecular structure of triple helical recombinant collagen (THRC) enriched with amino groups, creating an auspicious condition for the occurrence of crosslinking reactions. The formation of PEG-ChS-THRC hydrogel was masterminded through the orchestrated covalent crosslinking of amino groups in ChS-ADH and THRC with N-hydroxysuccinimide (NHS) in polyethylene glycol active ester (NHS-PEG-NHS). The resulting hydrogel offered advantageous structural support at the site of cranial defects, while also exhibiting remarkable bioactivity attributable to the incorporation of THRC. Ultimately, the bioactive PEG-ChS-THRC hydrogel substantially facilitated the regeneration of bone tissue, providing a significant therapeutic avenue for addressing cranial defects.

3.2 Characterization of THRC and ChS-ADH

The purity and structural integrity of THRC were evaluated using SDS-PAGE analysis and circular dichroism (CD) spectra. The SDS-PAGE image displayed a distinct and well-defined band within the 25–35 kDa range

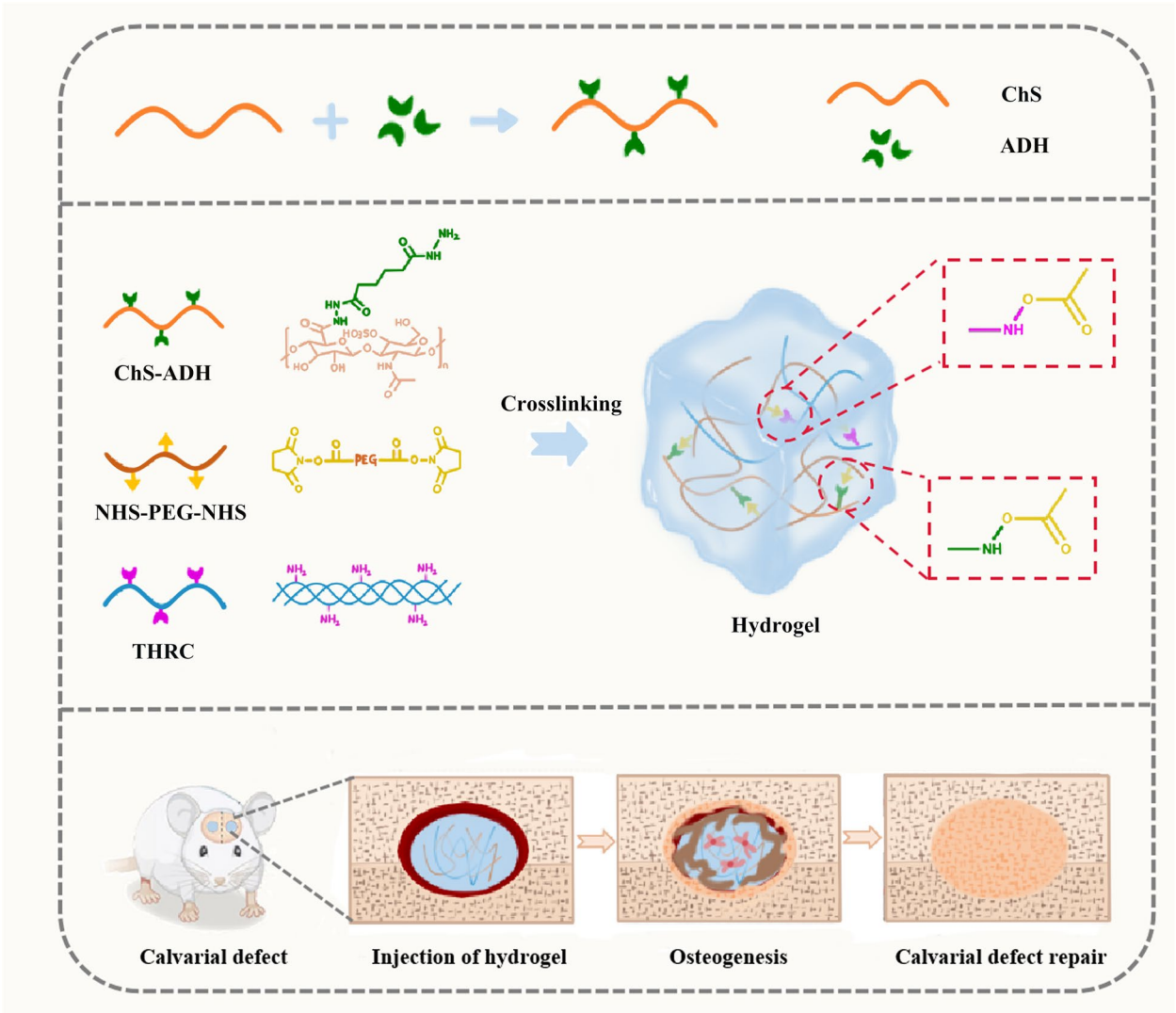

Fig. 1 Schematic design of a bioactive PEG-ChS-THRC hydrogel for enhanced cranial defect repair in rats

for the THRC sample (Fig. 2A), affirming the successful preparation of a highly pure THRC. The CD spectra of THRC exhibited a characteristic peak at 222 nm and revealed a melting temperature (Tm) of 33.8 °C (Fig. 2B-D), providing evidence for the formation of a stable triple-helical structure in the THRC.

The substitution degree of ChS-ADH was analyzed by ^{1}H NMR spectroscopy. The ^{1}H NMR spectra of ChS exhibited a typical peak at 1.81 ppm (peak a, assigned to the -CH_3 group), along with multiple peaks spanning 3.25–4.65 ppm (peak f, assigned to the protons in the ChS sugar ring). Meanwhile, distinctive peaks at 2.15 ppm (peaks b, c, assigned to the -CH_2 group) and 1.40 ppm (peaks d, e, assigned to the -CH_2 group) were discerned in ADH (Fig. S1). Notably, the ChS-ADH showcased corresponding peaks of both ChS (peaks a and f) and ADH (peaks b, c, and d, e), indicating the successful conjugation of ADH and ChS (Fig. 2E). The modification level of ChS-ADH was calculated to be 72%, which was quantitatively estimated by the integration ratio between the methylene in ADH (peaks b, c, and d, e) and the N-acetyl group in ChS (peak a).

3.3 Synthesis and characterization of PEG-ChS-THRC hydrogel

The synthesis of PEG-ChS-THRC hydrogel was performed through a straightforward approach under mild conditions. Initially, the stock solutions of NHS-PEG-NHS (160 mg/mL) and ChS-ADH (100 mg/mL) were prepared in 0.9% saline, respectively. Subsequently, 20 mg, 40 mg and 80 mg of THRC were added to the 500 µL of ChS-ADH solution to create a series of mixtures. Ultimately, 500 µL of the NHS-PEG-NHS were blended with each mixture, culminating in the formation of PEG-ChS-$THRC_{10}$, PEG-ChS-$THRC_{20}$, and PEG-ChS-$THRC_{40}$ hydrogels.

The morphology of PEG-ChS-THRC hydrogels at varying concentrations of THRC was characterized by scanning electron microscope (SEM). The images of the lyophilized PEG-ChS and PEG-ChS-THRC hydrogels displayed a three-dimensional interconnected porous network with unevenly distributed pores (Fig. 3A-D). The pore sizes of PEG-ChS, PEG-ChS-$THRC_{10}$, PEG-ChS-$THRC_{20}$, and PEG-ChS-$THRC_{40}$ hydrogels were calculated as 4.8 ± 0.5 µm, 5.7 ± 0.4 µm, 7.4 ± 0.6 µm, and 6.4 ± 0.7 µm, respectively (Fig. 3E). The introduction of THRC resulted in an enlargement of the pore size in the PEG-ChS-THRC hydrogel, facilitating cellular growth and nutrient circulation. The results indicated that the inclusion of THRC effectively modulated the porous structure of the PEG-ChS-THRC hydrogel.

Fourier transform infrared spectroscopy (FT-IR) was recorded to examine the crosslinking of NHS-PEG-NHS, ChS-ADH and THRC (Fig. 3F). A distinct vibration peak of THRC at 1658 cm^{-1} and 1550 cm^{-1} was corresponded to the C=O bond. FT-IR spectra of ChS-ADH displayed typical peaks at 1415 cm^{-1} attributed to C-O bond, and 1654 cm^{-1} and 1576 cm^{-1} ascribed to C=O bond. A characteristic vibration peak at 2888 cm^{-1} and 1738 cm^{-1} was exhibited in FT-IR spectra of PEG, assigned to -CH_2 and C=O bond. Notably, the FT-IR spectra of the PEG-ChS-THRC hydrogel showed vibration peaks at 2888 cm^{-1} and 1738 cm^{-1} (-CH_2 and C=O groups from PEG), 1658 cm^{-1} and 1550 cm^{-1}(C=O group from THRC and ChS-ADH), 1415 cm^{-1} (C-O bond from ChS-ADH). These results suggested that the PEG-ChS-THRC

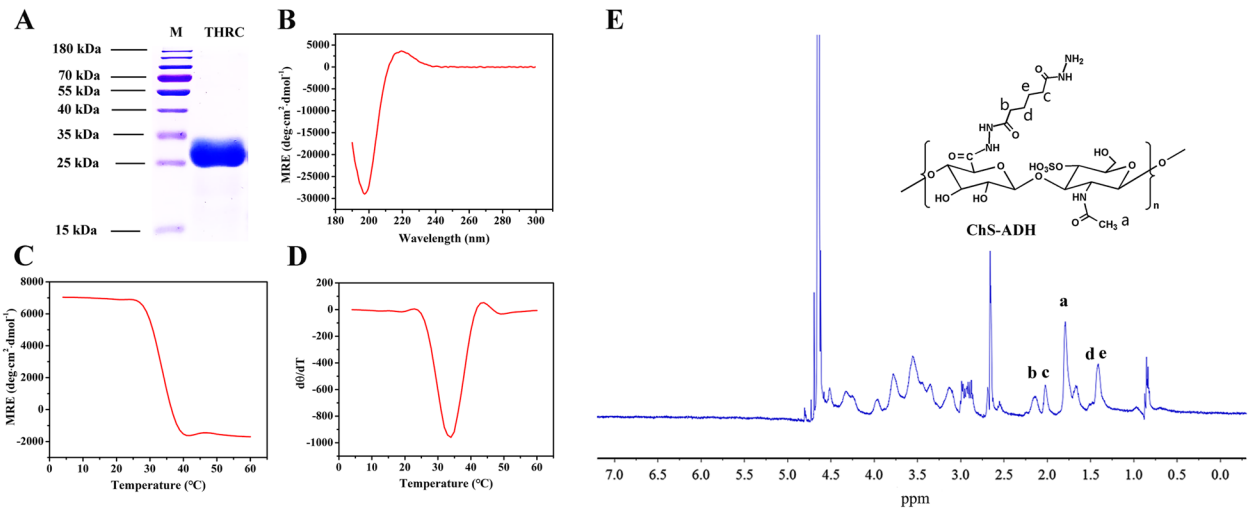

Fig. 2 Characterization of THRC and ChS-ADH. **A** SDS-PAGE image of THRC; **B** CD wavelength scans, **C** thermal transition, and (**D**) the first derivative (dθ/dT) of the thermal transition curves; **E** ^{1}H NMR spectra of ChS-ADH

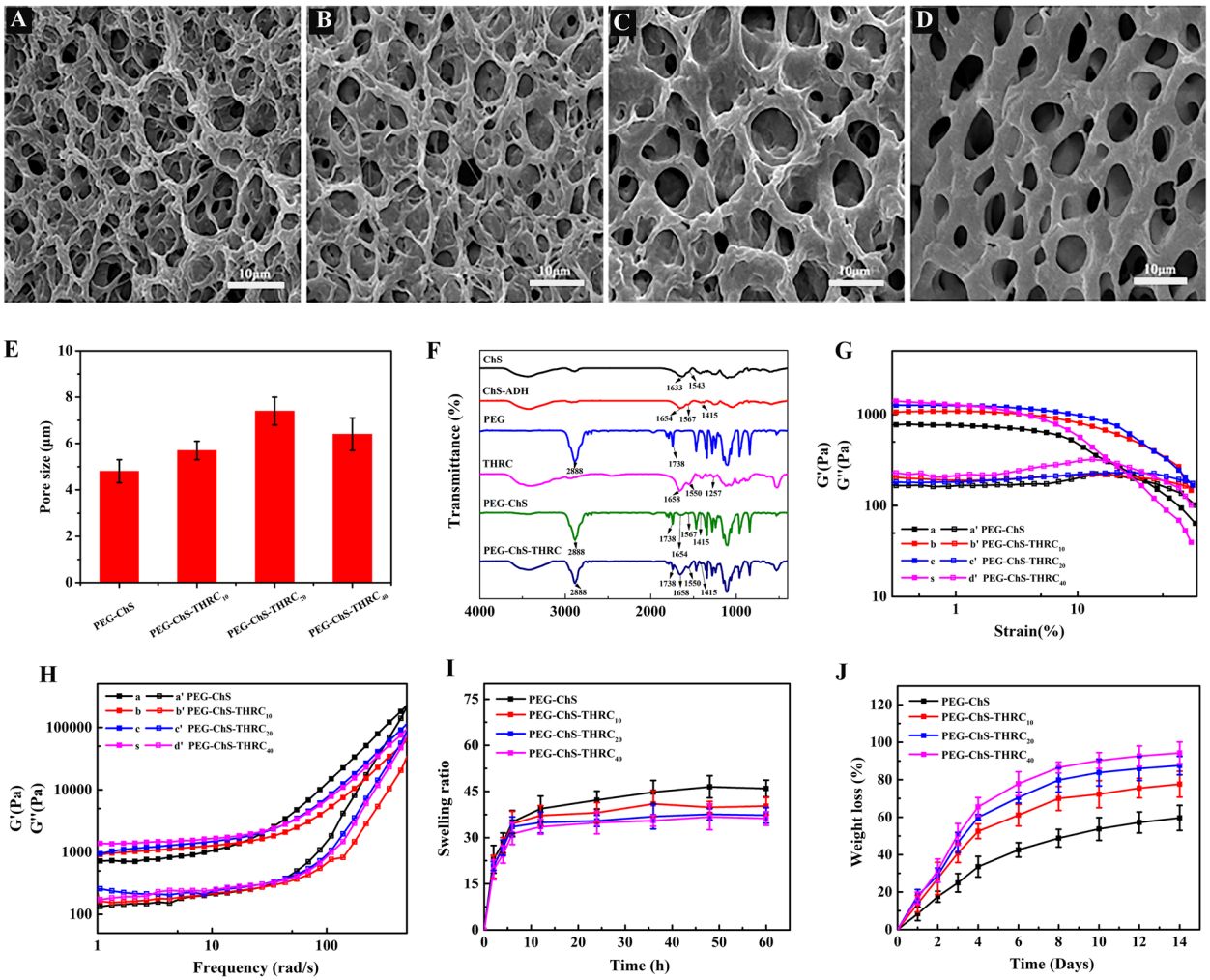

Fig. 3 Characterization of PEG-ChS-THRC hydrogels. SEM of (**A**) PEG-ChS, **B** PEG-ChS-THRC$_{10}$, **C** PEG-ChS-THRC$_{20}$, and (**D**) PEG-ChS-THRC$_{40}$ hydrogels; **E** Pore sizes calculated by SEM; **F** FT-IR; **G** Strain-dependent and **H** frequency-dependent oscillatory shear rheology; **I** Swelling property and (**J**) collagenase degradation of hydrogels

hydrogel was fabricated through crosslinking of NHS-PEG-NHS, ChS-ADH and THRC.

The mechanical properties of the hydrogels were assessed through rheological analysis, measuring their storage modulus (G') and loss modulus (G"). Strain-dependent oscillatory rheology demonstrated that the critical strain values at gel-sol transition point were approximately 35.8%, 85.5%, 87.8% and 21.2% for the PEG-ChS, PEG-ChS-THRC$_{10}$, PEG-ChS-THRC$_{20}$, and PEG-ChS-THRC$_{40}$ hydrogels, respectively (Fig. 3G). Frequency-dependent oscillatory shear rheology manifested the dominance of G′ values, measuring approximately 769.7 Pa, 1078.3 Pa, 1261.1 Pa, and 1346.8 Pa for all four hydrogels, respectively (Fig. 3H). These results underscored significantly enhanced mechanical strength of PEG-ChS-THRC hydrogel with the increased concentration of THRC.

The swelling ratio (SR) of lyophilized hydrogels was examined through immersion in PBS solutions (Fig. 3I). The SR of the PEG-ChS, PEG-ChS-THRC$_{10}$, PEG-ChS-THRC$_{20}$, and PEG-ChS-THRC$_{40}$ hydrogels demonstrated a gradual augmentation, attaining equilibrium after approximately 48 h. The final values of swelling equilibrium were determined as 46.0, 40.3, 37.3, and 36.2, respectively. These results highlighted diminished swelling ratios of the PEG-ChS-THRC hydrogels as the concentrations of THRC increased.

The in vitro degradation of freeze-dried hydrogels was investigated in collagenase solutions (Fig. 3J). After incubation of 14 days, the degradation rates of PEG-ChS, PEG-ChS-THRC$_{10}$, PEG-ChS-THRC$_{20}$, and PEG-ChS-THRC$_{40}$ hydrogels were calculated as 59.63%, 77.65%, 87.55%, and 94.26%, respectively. Notably, the PEG-ChS-THRC$_{40}$ hydrogel manifested a markedly accelerated

collagenase degradation attributable to the heightened concentration of THRC. The results demonstrated that the introduction of THRC endowed the PEG-ChS-THRC hydrogel with adjustable biodegradability.

3.4 Biocompatibility and bioactivity of PEG-ChS-THRC hydrogel

The in vitro cytotoxicity of PEG-ChS and PEG-ChS-THRC hydrogels was assessed by examining the viability of rat bone marrow mesenchymal stem cells (rBMSCs) through CCK-8 assays (Fig. 4A). Following a 24-hour incubation period, the cell viability for the PEG-ChS and PEG-ChS-THRC groups was determined to be 118% and 133%, respectively. These results suggested that the PEG-ChS-THRC hydrogel possessed notable biocompatibility.

The cell proliferation of PEG-ChS-THRC hydrogel was evaluated utilizing the cell counting kit-8 (CCK-8) assay. The cell viability of ChS, THRC, PEG-ChS, and PEG-ChS-THRC groups exhibited a time-dependent augmentation following incubation from 1 to 7 days. Remarkably, the density of viable cells was markedly higher in the PEG-ChS-THRC hydrogel compared to that of the ChS, THRC, and PEG-ChS groups (Fig. 4B). Furthermore, the CCK-8 assays revealed a progressive increase in the cell numbers of the PEG-ChS-THRC hydrogel with escalating concentrations of THRC (Fig. 4C). These results underscored the exceptional biocompatibility of the PEG-ChS-THRC hydrogel, which significantly expedited cell proliferation.

Cellular adhesion of BMSCs cultured with ChS, THRC, PEG-ChS, and PEG-ChS-THRC were examined utilizing immunofluorescence staining. A small amount of BMSCs with suboptimal cytoskeletal structures were observed in the Blank and ChS, while the THRC and PEG-ChS displayed well-developed cytoskeletal structures. Notably, an increasing number of BMSCs adhered to the

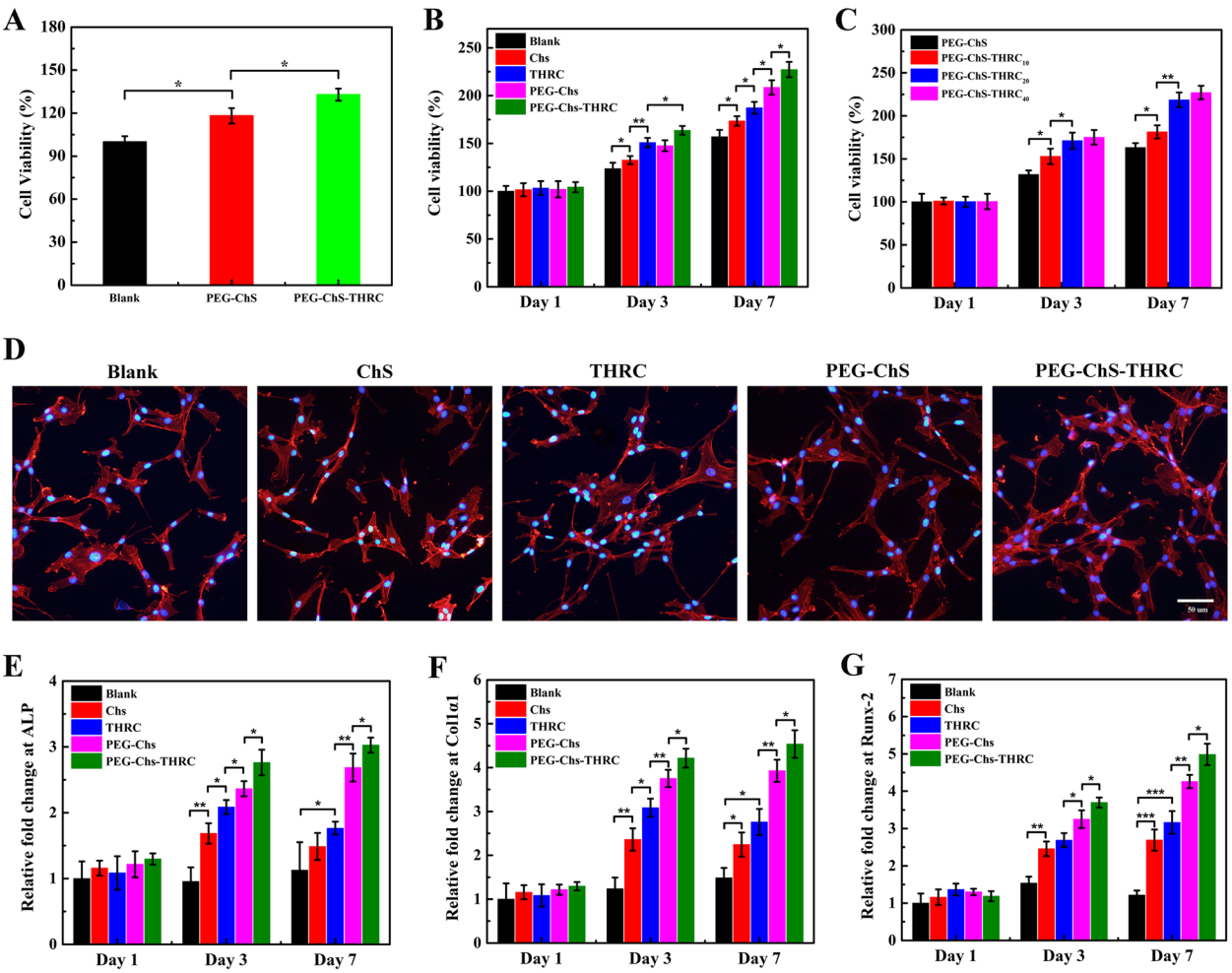

Fig. 4 Biocompatibility and bioactivity of PEG-ChS-THRC hydrogels in vitro. **A** In vitro cytotoxicity of the PEG-ChS and PEG-ChS-THRC hydrogels; Cell proliferation of (**B**) ChS, THRC, PEG-ChS, and PEG-ChS-THRC, and (**C**) PEG-ChS, PEG-ChS-THRC$_{10}$, PEG-ChS-THRC$_{20}$, and PEG-ChS-THRC$_{40}$; **D** Immuno- fluorescence staining; The relative expression levels of osteogenic specific gene (**E**) *ALP*, (**F**) *Col1a1*, and (**G**) *Runx-2*

PEG-ChS-THRC hydrogel, showcasing exquisite actin cytoskeletal arrangements (Fig. 4D). The results indicated that PEG-ChS-THRC hydrogel provided bioactive scaffolds, effectively promoting the adhesion of BMSCs.

A cellular motility assessment was conducted via a migration assay (Fig. S2). Following a 24-hour co-culture period of the extract with BMSCs, the blank group displayed a cell migration rate of 10.8%, whereas the values of ChS, THRC, and PEG-ChS groups were determined to be 24.2%, 33.8%, and 41.1%, respectively. Notably, the PEG-ChS-THRC group demonstrated a remarkable cellular migration rate of 83.1%. These results highlighted the substantial enhancement of BMSCs' migratory capacity by the PEG-ChS-THRC hydrogel.

The expression of critical osteogenic marker genes of BMSCs were further evaluated by real time-quantitative polymerase chain reaction (RT-qPCR) analysis (Fig. 4E-G). Following a 7-day incubation, the PEG-ChS group exhibited increased expression levels of *ALP*, *Col1a1*, and *Runx-2* genes compared to the ChS and THRC groups, credited to the supportive nature of hydrogel scaffolds. Remarkably, the PEG-ChS-THRC group demonstrated significantly heightened expression of osteogenic-specific genes compared to the PEG-ChS group, attributed to the introduction of bioactive THRC. These results signified the exceptional bioactivity of the PEG-ChS-THRC hydrogel, which remarkably enhanced the osteogenic differentiation of BMSCs.

3.5 CT and MRI analysis for bone regeneration

A critical-sized cranial defect model in rats was established to explore the efficacy of promoting bone regeneration. After the rats were anesthetized, two 5 mm diameter cranial defect was drilled, and then each hydrogel was placed on top of the endocranium and allowed to fill the two defect completely (Fig. 5A). The bone regeneration abilities of the hydrogels were investigated after implantation for 2 weeks, 4 weeks and 8 weeks.

Computed tomography (CT) was performed to evaluate the capacity for repairing cranial defect (Fig. 5B). The CT images of the blank group revealed minimal formation of new bone at the defect sites after 56 days, confirming the absence of inherent self-healing ability in critical-size cranial defects. The PEG-ChS treated group manifested a decrease in the area of cranial defects, while the PEG-ChS-THRC group demonstrated a significantly smaller defect area (Fig. 5C). The results suggested that the PEG-ChS-THRC hydrogels markedly enhanced bone regeneration capability.

Magnetic resonance imaging (MRI) was employed to further examine the cranial bone regeneration (Fig. 6). At the first day, the blank, PEG-ChS and PEG-ChS-THRC groups showcased a substantial segment lacking low T1 signal, indicating the presence of significant bone defects. Meanwhile, the high signal of T2 may be attributed not only to the hydrogels but also to tissue edema and encephalocele (Fig. 6A-C). At the 56th day, the blank group displayed a notable fragment without low T1 signal, whereas the PEG-ChS treated group showed a small central segment with low T1 signal. Notably, the PEG-ChS-THRC treated group demonstrated continuous low T1 signal as well as significantly stronger and broader low signals of T2 (Fig. 6D-F), suggesting a greater formation of bone tissue within the cranial defects.

3.6 Histological analysis

The hydrogels-mediated bone regeneration was further investigated by hematoxylin and eosin (H&E). At 14 days, a significantly larger quantity of hydrogel persisted in the PEG-ChS treated group, suggesting its inadequate degradation in vivo (Fig. 7A, D). At 28 days, the PEG-ChS-THRC treated group displayed a notable presence of pink osteoid, representing fibrous tissue situated further from the original bone tissues. In contrast, the PEG-ChS treated group exhibited only a few pink osteoid (Fig. 7B, E). At 56 days, the PEG-ChS-THRC treated group showed a substantial increase of regenerated bone tissues, while a comparatively lesser amount of newly formed bone was observed in the PEG-ChS treated group (Fig. 7C, F). The H&E staining revealed that the PEG-ChS-THRC hydrogel possessed favourable biodegradability and remarkable osteogenic activity, accelerating bone tissue regeneration and cranial defect repair.

3.7 Mechanism of PEG-ChS-THRC hydrogel for cranial defect repair

A bioactive PEG-ChS-THRC hydrogel has been synthesized for the treatment of cranial defects. The formation of the PEG-ChS-THRC hydrogel was orchestrated through the covalent crosslinking of amino groups in ChS-ADH and THRC with N-hydroxysuccinimide (NHS) in polyethylene glycol active ester (NHS-PEG-NHS). Incorporating THRC effectively increased the pore size of the PEG-ChS-THRC hydrogel, facilitating cell growth and nutrient circulation. Compared to PEG-ChS, the PEG-ChS-THRC hydrogel exhibited significantly enhanced mechanical strength, providing substantial structural support for cell growth. Additionally, the PEG-ChS-THRC hydrogel displayed reduced swelling ratios and a notable degradation rate with increasing concentrations of THRC, which would promote cranial bone tissue regeneration.

Cell experiments consistently demonstrated that the PEG-ChS-THRC hydrogel effectively promoted cell proliferation, adhesion, and osteogenic differentiation due to its remarkable characteristics. Upon

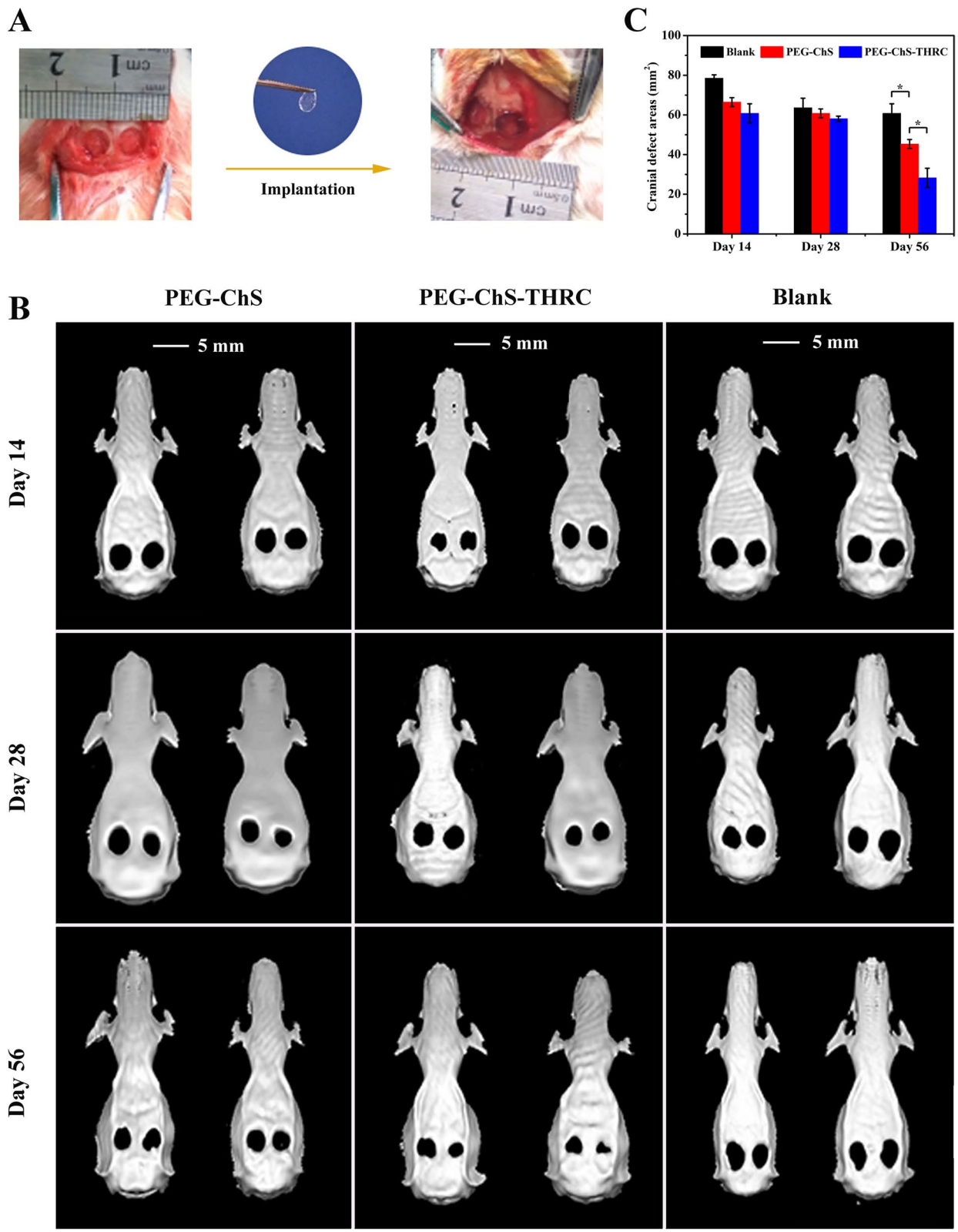

Fig. 5 **A** Cranial defect model construction and in vivo implantation, **B** CT images, and **C** changes of cranial defects post implantation of Blank, PEG-ChS and PEG-ChS-THRC

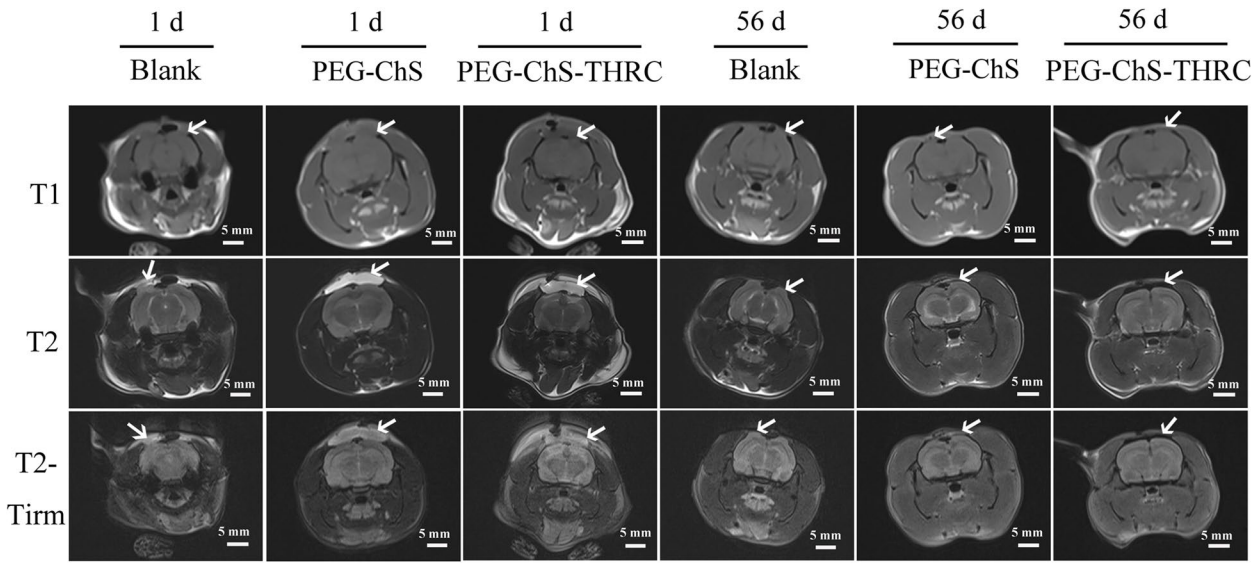

Fig. 6 MRI T1, T2 and T2-Tirm images of cranial defects post implantation of PEG-ChS hydrogel, PEG-ChS-THRC hydrogel, and the Blank group. The measurements were performed at 1 day and 56 days after implantation

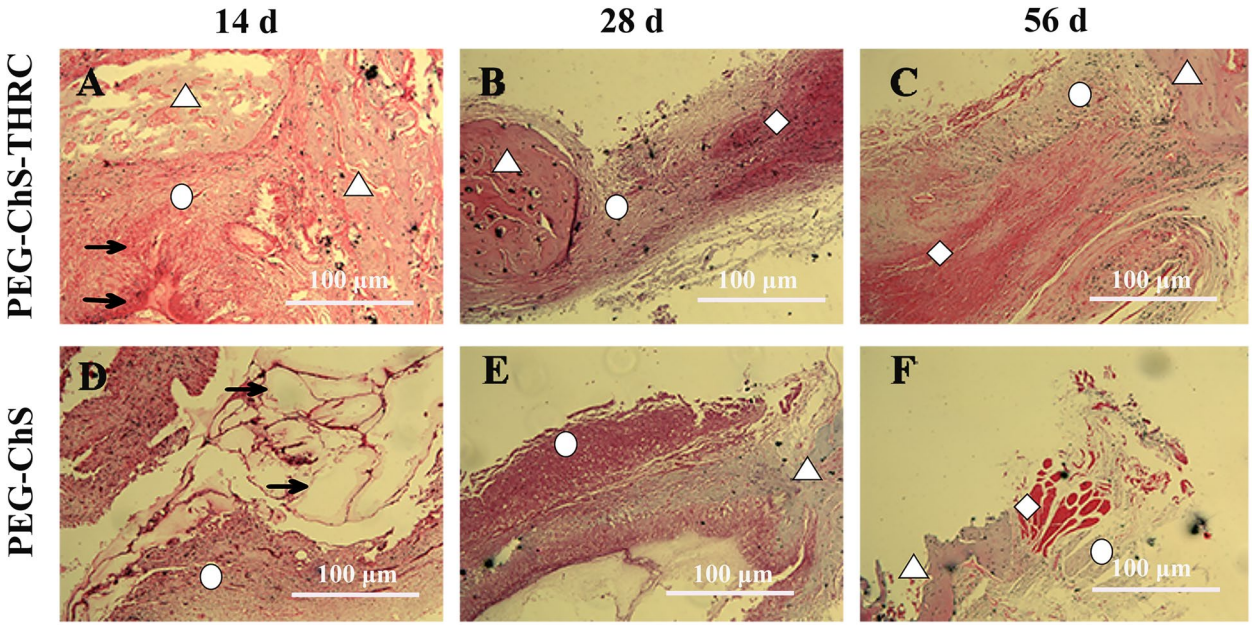

Fig. 7 H&E staining of rat cranial tissue sections post implantation of PEG-ChS hydrogels and PEG-ChS-THRC hydrogels. (→) Undegraded hydrogels, (○) Tissue bands, (△) Original bone tissues, (◇) New bone tissues

implantation into cranial defects, this hydrogel not only offered favorable support but also exhibited remarkable biocompatibility, bioactivity, and appropriate biodegradation. Ultimately, the bioactive PEG-ChS-THRC hydrogel significantly enhanced bone tissue regeneration, presenting a promising strategy for cranial defect treatment.

3.8 The potential limitations and future directions

While considerable strides have been made in this work, it is essential to acknowledge the persistence of potential limitations. Firstly, recombinant collagen offers notable

advantages over animal-derived collagen, particularly in terms of its non-immunogenic nature and diminished susceptibility to viral infection. Nevertheless, it is paramount to emphasize the necessity for additional validation through pivotal experiments such as immunogenicity assays and viral detection. These investigations are indispensable for ascertaining the safety and efficacy of recombinant collagen across a spectrum of biomedical applications.

Secondly, delving into the in vivo biodegradation of PEG-ChS-THRC hydrogel and discerning its degradation products constitute pivotal strides in evaluating its safety and efficacy for clinical translation. Employing biochemical assays, researchers can meticulously quantify the concentrations of specific degradation byproducts in biological specimens, yielding invaluable insights into degradation kinetics and pathways. Furthermore, histological scrutiny facilitates the visualization of tissue responses and the presence of degradation byproducts, thereby furnishing complementary data on in vivo biodegradation processes.

Thirdly, the heightened bioactivity witnessed in cranial defect repair with PEG-ChS-THRC hydrogel underscores its potential for applications in regenerative medicine. Nonetheless, the augmentation of its biological activity can be further realized through the integration of inorganic components and growth factors. Bioactive ceramics, as inorganic constituents, confer structural reinforcement and foster osteogenic differentiation, thereby fostering bone regeneration. Moreover, growth factors, such as bone morphogenetic proteins (BMPs) or platelet-derived growth factors (PDGFs), expedite tissue repair and bolster the development of functional tissue.

4 Conclusion

The rejuvenation of critical-size cranial defects presents an overwhelming challenge in tissue engineering. Herein, we have for the first time developed a bioactive poly(ethylene glycol)-chondroitin sulfate-triple helical recombinant collagen (PEG-ChS-THRC) hydrogel for enhanced cranial defects repair. A simple crosslinking strategy with mild conditions was utilized to fabricate the PEG-ChS-THRC hydrogel. The hydrogel exhibites interconnected porous structures, augmented mechanical strength, reduced swelling ratios, and customizable biodegradability, as well as pronounced biocompatibility and bioactivity, substantially promoting the proliferation, adhesion, migration and osteogenic differentiation of BMSCs. The results of rat models of critical-size cranial defects displays that the PEG-ChS-THRC hydrogel significantly facilitates bone tissue regeneration at 56 days post implantation. Notably, the PEG-ChS-THRC hydrogel demonstrated the effectively improved bone regeneration capability and excellent degradation performance compared with PEG-ChS hydrogel, which would be attributed to the addition of THRC. The bioactive PEG-ChS-THRC hydrogel provides a supreme remedy of critical-size cranial defects, holding great potential in bone tissue engineering and regenerative medicine.

Supplementary Information

The online version contains supplementary material available at https://doi.org/10.1186/s42825-024-00168-4.

Supplementary Material 1.

Acknowledgements
The authors gratefully acknowledge the financial support from the National Natural Science Foundation of China (grant nos. 22074057, 21775059 and 21305056).

Authors' contributions
WL designed this project and wrote the original draft. ZS and YF performed experiments. CX and HH analyzed data and draw the scheme. LZ and XJ reviewed and edited the manuscript.

Funding
This work was supported by grants from the National Natural Science Foundation of China (grant nos. 22074057, 21775059 and 21305056).

Availability of data and materials
Not applicable.

Declarations

Ethics approval and consent to participate
The animal study was approved by the Ethics Committee of the Lanzhou University No.1 Hospital (No. LDYYLL-2019-271). All the animals were purchased from Laboratory Animal Center of Lanzhou University and the animal certification is No. LZU-SD-1206-30. The animal experiment guidance from the ethical committee and the guide for care and use of laboratory animals from NIH were followed during the whole experiment course.

Competing interests
The authors declare no competing conflict of interest.

Author details
[1]State Key Laboratory of Applied Organic Chemistry, College of Chemistry and Chemical Engineering, Lanzhou University, Lanzhou 730000, China. [2]Gansu Engineering Research Center of Medical Collagen, Lanzhou 730000, China. [3]Joint Research Center of Collagen of Lanzhou University-China National Biotec Group.-Lanzhou Biotechnology Development Co., Lanzhou 730000, China. [4]School of Chemical and Biological Engineering, Lanzhou Jiaotong University, Lanzhou 730070, China.

Received: 8 December 2023 Revised: 5 May 2024 Accepted: 22 May 2024
Published online: 01 August 2024

References

1. Lee JC, Volpicelli EJ. Bioinspired collagen scaffolds in cranial bone regeneration: from bedside to bench. Adv Healthc Mater. 2017;6:1700232.
2. Lu GG, Xu Y, Liu QY, Chen MY, Sun H, Wang PL, Li X, Wang YX, Li X, Hui XH, Luo E, Liu J, Jiang Q, Liang J, Fan YJ, Sun Y, Zhang XD. An instantly fixable and self-adaptive scaffold for skull regeneration by autologous stem cell recruitment and angiogenesis. Nat Commun. 2022;13:2499.
3. Tan L, Hu Y, Li MH, Zhang YC, Xue CC, Chen MH, Luo Z, Cai KY. Remotely-activatable extracellular matrix-mimetic hydrogel promotes physiological

bone mineralization for enhanced cranial defect healing. Chem Eng J. 2022;431:133382.
4. Hosseini FS, Abedini AA, Chen F, Whitfield T, Ude CC, Laurencin CT. Oxygen-generating biomaterials for translational bone regenerative engineering. ACS Appl Mater Interfaces. 2023;15:50721–41.
5. Pape HC, Evans A, Kobbe P. Autologous bone graft: properties and techniques. J Orthop Trauma. 2010;24(Suppl 1):S36–40.
6. Sharifi M, Kheradmandi R, Salehi M, Alizadeh M, Ten Hagen TLM, Falahati M, Criteria. Challenges, and opportunities for acellularized allogeneic/xenogeneic bone grafts in bone repairing. ACS Biomater Sci Eng. 2022;8:3199–219.
7. Xu H, Niu CS, Fu XM, Ding WH, Ling SY, Jiang XF, Ji Y. Early cranioplasty vs. late cranioplasty for the treatment of cranial defect: a systematic review. Clin Neurol Neurosur. 2015;136:33–40.
8. Cui ZK, Kim S, Baljon JJ, Wu BM, Aghaloo T, Lee M. Microporous methacrylated glycol chitosan-montmorillonite nanocomposite hydrogel for bone tissue engineering. Nat Commun. 2019;10:3523.
9. Chen Z, Lv Y. Gelatin/sodium alginate composite hydrogel with dynamic matrix stiffening ability for bone regeneration. Compos B Eng. 2022;243:110162.
10. Jiang LB, Su DH, Ding SL, Zhang QC, Li ZF, Chen FC, Ding W, Zhang ST, Dong J. Salt-assisted toughening of protein hydrogel with controlled degradation for bone regeneration. Adv Funct Mater. 2019;29:1901314 C.
11. Fu SL, Dong H, Deng XY, Zhuo RX, Zhong ZL. Injectable hyaluronic acid/poly(ethylene glycol) hydrogels crosslinked via strain-promoted azide-alkyne cycloaddition click reaction. Carbohyd Polym. 2017;169:332–40.
12. Ge P, Cai Q, Zhang H, Yao X, Zhu W. Full poly(ethylene glycol) hydrogels with high ductility and self-recoverability. ACS Appl Mater Interfaces. 2020;12:37549–60.
13. Xu F, Tan F, Zheng ZR, Zhou XW. Effects of pre-osteogenic differentiation on the bone regeneration potentiality of marrow mesenchymal stem cells/poly (ethylene glycol)-diacrylate hydrogel using a rat cranial defect model. J Biomater Appl. 2022;37:786–94.
14. Ai YL, She WT, Wu SY, Shao Q, Jiang ZR, Chen PC, Mei L, Zou C, Peng YJ, He Y. AM1241-loaded poly (ethylene glycol)-dithiothreitol hydrogel repairs cranial bone defects by promoting vascular endothelial growth factor and COL-1 expression. Front Cell Dev Biol. 2022;10:888598.
15. Lü SY, Bai X, Liu HD, Ning P, Wang ZQ, Gao CM, Ni BL, Liu MZ. An injectable and self-healing hydrogel with covalent cross-linking in vivo for cranial bone repair. J Mater Chem B. 2017;5:3739–48.
16. Bai X, Lü SY, Liu HD, Cao Z, Ning P, Wang ZQ, Gao CM, Ni BL, Ma DY, Liu MZ. Polysaccharides based injectable hydrogel compositing bio-glass for cranial bone repair. Carbohydr Polym. 2017;175:557–64.
17. Pal P, Tucci MA, Fan LW, Bollavarapu R, Lee JW, Marocho SMS, Janorkar AV. Functionalized collagen/elastin-like polypeptide hydrogels for craniofacial bone regeneration. Adv Healthc Mater. 2022;12:2202477.
18. Zhang TT, Chen H, Zhang YJ, Zan Y, Ni TY, Liu M, Pei RJ. Photo-crosslinkable, bone marrow-derived mesenchymal stem cells- encapsulating hydrogel based on collagen for osteogenic differentiation. Colloid Surf B. 2019;174:528–35.
19. Chen L, Wu CH, Chen SP, Zhang YS, Liu A, Ding J, Wei D, Guo ZZ, Sun J, Fan HS. Biomimetic mineralizable collagen hydrogels for dynamic bone matrix formation to promote osteogenesis. J Mater Chem B. 2020;8:3064–75.
20. Wang J, Hu JY, Yuan X, Li YN, Song LJ, Xu F. Recombinant collagen hydrogels induced by disulfide bonds. J Biomed Mater Res A. 2022;110:1774–85.
21. Tytgat L, Dobos A, Markovic M, Van Damme L, Van Hoorick J, Bray F, Thienpont H, Ottevaere H, Dubruel P, Ovsianikov A, Van Vlierberghe S. High-resolution 3D bioprinting of photo-cross-linkable recombinant collagen to serve tissue engineering applications. Biomacromolecules. 2020;21:3997–4007.
22. Fang ZY, Lu C, Du WJ, Wang X, Yang HY, Shi MJ, Liu TT, Xie YJ, Wang SF, Xu XB, Li HH, Wang HB, Zheng YD. Injectable self-assembled dual-crosslinked alginate/recombinant collagen-based hydrogel for endometrium regeneration. Int J Biol Macromol. 2023;236:123943.
23. Yoshizumi A, Yu Z, Silva T, Thiagarajan G, Ramshaw JA, Inouye M, Brodsky B. Self-association of streptococcus pyogenes collagen-like constructs into higher order structures. Protein Sci. 2009;18:1241–51.
24. Liu MR, Du HL, Zhai GX. Self-assembled nanoparticles based on chondroitin sulfate-deoxycholic acid conjugates for docetaxel delivery: Effect of degree of substitution of deoxycholic acid. Colloid Surf B. 2016;146:235–44.

Publisher's Note